PCCP

Accepted Manuscript

ROYAL SOCIETY OF CHEMISTRY

www.rsc.org/pccp

Cite this: DOI: 10.1039/c0xx00000x

www.rsc.org/xxxxxx

ARTICLE TYPE

Electronic structure and electrode properties of tetracyanoquinodimethane (TCNQ): A surface science investigation of lithium intercalation into TCNQ

Ruben Precht,* René Hausbrand and Wolfram Jaegermann

Received (in XXX, XXX) Xth XXXXXXXXX 20XX, Accepted Xth XXXXXXXXX 20XX
DOI: 10.1039/b000000x

Organic materials are of interest as ion battery cathode materials because they offer advantages over inorganic cathodes such as abundant resources and a low ecological footprint. However, they suffer from slow kinetics and a comparatively low potential. In this paper, we have investigated alkali induced changes in the electronic structure of tetracyanoquinodimethane (TCNQ) to be used as cathode material in Li-ion batteries. Lithium was inserted stepwise into TCNQ thin films by exposure to lithium vapour and analysis by photoemission (PES) was performed. The evolution of core levels, electronic structure and Fermi-level with increasing lithium insertion into TCNQ was monitored. The results show that lithium insertion takes place under integer charge transfer and polaron formation. We find no indication of deterioration of the material. The consequences of evolution of electronic structure and polaron formation for electrode potential and kinetic properties of the material are discussed.

1. Introduction

Organic materials have been investigated for some time regarding their application in lithium batteries [1]. They are transition-metal free and offer the advantage of abundant resources and low ecological footprint [2,3], but suffer from slow kinetics and a comparatively low potential. Investigations have been performed on various organic lithium insertion cathode materials, such as polypyrole and tetracyanoquinodimethane (TCNQ) [1,2,4,5], some of them with very promising results. With a TCNQ composite electrode a specific capacity of 263 mAh/g [2] could be reached with flat shaped charge-discharge curves [2,6].

During intercalation of lithium into a host material, lithium ions are incorporated at suitable locations in the host and electrons fill unoccupied electronic states of the host. Upon intercalation, i.e. as a result of the intercalation reaction, the electronic structure of the host undergoes changes, with consequences for potential and stability of the material. For inorganic materials these changes are generally moderate over quite a wide composition range [7,8], while for organic materials more pronounced changes take place due to polaron formation upon the accommodation of excess electrons [9]. The potential of an insertion electrode depends on the electron chemical potential (Fermi level) of the electrode material as well as the electric potential drop at the electrode-electrolyte interface, related to the chemical potential of guest ions in the electrode. It is generally accepted that the position of the Fermi level is the dominating factor [10] (see also [8]) and consequently electrode potentials (and cell voltages) reflect in first instance the position of the Fermi level(s) in the electrode(s). Therefore, investigations of electronic structure evolution with the degree of insertion and of related Fermi level shifts shed light on the value of cell voltage and specifically on the shape of (equilibrium) charge-discharge curves. Also, kinetic and stability aspects may be addressed.

In the past, the electronic structure and electronic properties of conducting organic materials and their interfaces have been explored mainly in the context of organic light emitting diodes (OLEDs), organic field-effect transistors (OFETs), or similar devices (see e.g. [11,12]). The consequences of polaron formation for the electrode potential and interface resistance of organic materials as Li-ion battery electrodes have not been widely discussed, however.

Photoemission (PES) is a well known surface analysis technique which gives access to Fermi level and electronic structure of a material. Investigations using thin films allow dedicated analysis of bulk, surface and interface properties using surface science methodology [4,13]. In the field of ion batteries, surface science methodology has already been used to investigate the intercalation of alkali into inorganic host structures [14,15] and more recently to investigate electrode-electrolyte interfaces [16] In a typical insertion experiment, the host structure is exposed to alkali vapour and the electronic structure of the resulting alkali-containing material is analyzed with PES. Such experiments are typically performed stepwise in order to track gradual changes occurring upon alkali insertion.

In this contribution, we investigate the insertion of lithium into TCNQ and its effect on the electronic structure by means of such a surface science insertion experiment. We exposed TCNQ thin films step-by-step to increasing amounts of lithium vapour and monitored changes of composition and the electronic structure by X-ray photoelectron spectroscopy (XPS) and ultra-violet photo

Cite this: DOI: 10.1039/c0xx00000x

www.rsc.org/xxxxxx

ARTICLE TYPE

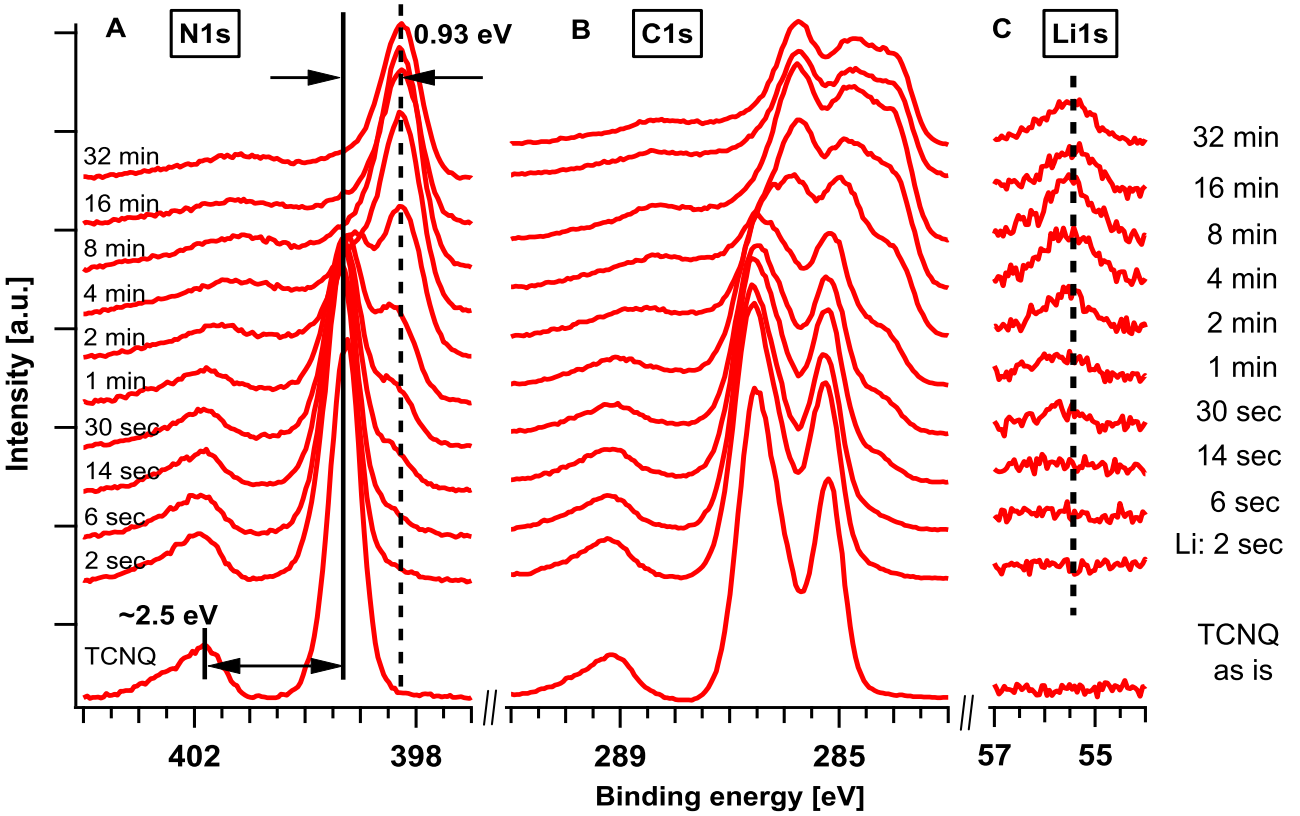

Fig. 1 XP spectra of N1s (A), C1s (B) and Li1s (C) during stepwise lithium intercalation. The bottom line represents pure TCNQ. The lines above are marked with the deposition time of lithium. The new N1s peak maximum is approximately 0.93 eV shifted to lower binding energies. Compared to N1s and C1s the Li1s peak does not shift during longer deposition times. Zero binding energy is referred to the Fermi level of a cleaned silver foil.

electron spectroscopy (UPS). We present the evolution of molecular structure, electronic structure and Fermi-level shifts with increasing lithium insertion into TCNQ and discuss the results with respect to use as insertion electrode.

2. Experimental

A TCNQ thin film (thickness ca. 20nm) was prepared onto an indium tin oxide substrate by evaporation of 7,7,8,8-TCNQ (98%, Sigma Aldrich Chemical) from an alumina crucible heated to 140°C. Subsequently, the film was stepwise exposed to lithium from a dispenser (SAES getters, current 7.5 A). After each step, the film was transferred back to the analysis chamber under vacuum conditions and analyzed by XPS and UPS. The pressure during lithium exposure was of $8 \cdot 10^{-8}$ mbar and no indication were found that any oxide was formed.

The experiment was performed in an integrated ultra-high vacuum (UHV) system (DArmstädter Integrated SYstem for SOLar cells, DAISY-SOL, base pressure $4 \cdot 10^{-9}$ mbar), which is equipped with a VG Escalab 250 photoelectron spectrometer. For XPS measurements a monochromatized Al-K_α X-ray source was used. The hemispherical photoelectron analyzer was operated with constant analyzer energy of 50 eV pass energy for survey spectra and 10 eV pass energy for detailed spectra with an energy resolution of about 400 meV. The spectrometer was calibrated to the Fermi edge and the core level lines of sputtered copper, silver and gold foils. Valence spectra have been measured with UPS using an excitation energy of He I (21.2 eV). The work function was determined by the secondary electron cut-off. For fitting the spectra Voigt functions and Shirley background were applied.

3. Results

3.1 XPS measurements

The C1s, N1s and Li1s XPS spectra of the exposure sequence are shown in Fig. 1. With increasing exposure time, additional components at lower binding energy both in the carbon and nitrogen XPS spectra are observed, indicating insertion of lithium and consecutive electron transfer to TCNQ molecules.

In case of the N1s spectrum the TCNQ film before deposition shows a single main component and a satellite 2.5 eV higher in binding energy. The single main component reflects the single

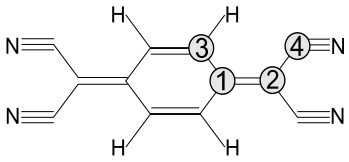

Fig. 2 Structure of TCNQ with four carbon atoms in different chemical environments.

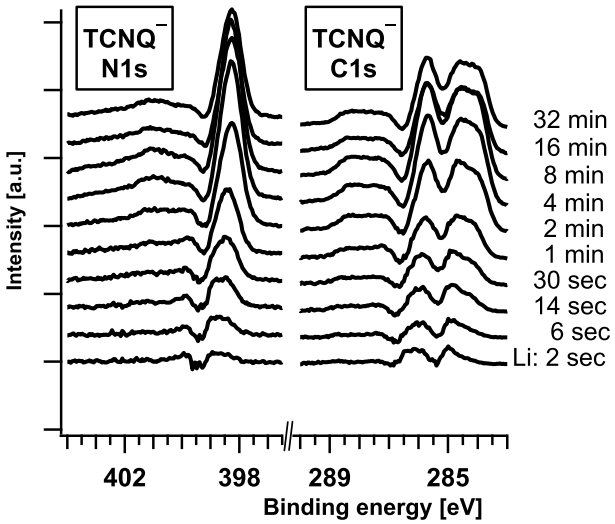

Fig. 3 XP spectra of N1s and C1s of negative charged component of $TCNQ^-$ during stepwise lithium intercalation. The bottom line representing pure TCNQ from Fig. 1 is not shown. The lines above are marked with the deposition time of lithium. The new N1s and C1s peak maxima both do not shift with continuing intercalation of lithium into TCNQ. The spectra are obtained by graphical subtraction of the pure from the intercalated TCNQ spectra in Fig. 1.

nitrogen component in the TCNQ molecule (see structure formula in Fig. 2) and the shake-up satellite electron excitation across the band gap in the semiconducting TCNQ. In the C1s spectrum, a double peak and a shake-up satellite is observed. In view of the four different carbon environments in the TCNQ molecule (see Fig. 2) four components can be expected. A fitting of the C1s peak is proposed in Fig. 10. In agreement to the N1s spectrum the satellite line due to bandgap excitation is found at a distance $\Delta E_G \sim 2.5$ eV.

The Li1s signal increases with exposure time and is characterized by a broad signal (in Fig. 1, C) at ca. 55.4 eV binding energy which is attributed to the formation of Li^+ according to literature values [14,17]. The formation of oxidic components could be excluded due to absence of O1s emission line.

Upon exposure a single new main component appears 0.93 eV lower in binding energy for the N1s spectrum. In case of the C1s spectrum multiple components appear at lower binding energy. By graphically subtracting the spectra of pure TCNQ from the spectra of lithiated TCNQ we obtain the N1s and C1s spectra of negatively charged TCNQ formed by electron transfer from lithium (see Fig. 3), which can be unambiguously distinguished from the spectra of TCNQ.

In the following, we denote these components to reduced "$TCNQ^-$". The actual unit exists as a biradical dimer $[TCNQ_2]^{2-}$ (see discussion for more details). Clearly, the amount of $TCNQ^-$ increases with exposure time. The C1s and N1s spectra of the exposure sequence look like a superposition of pure TCNQ and

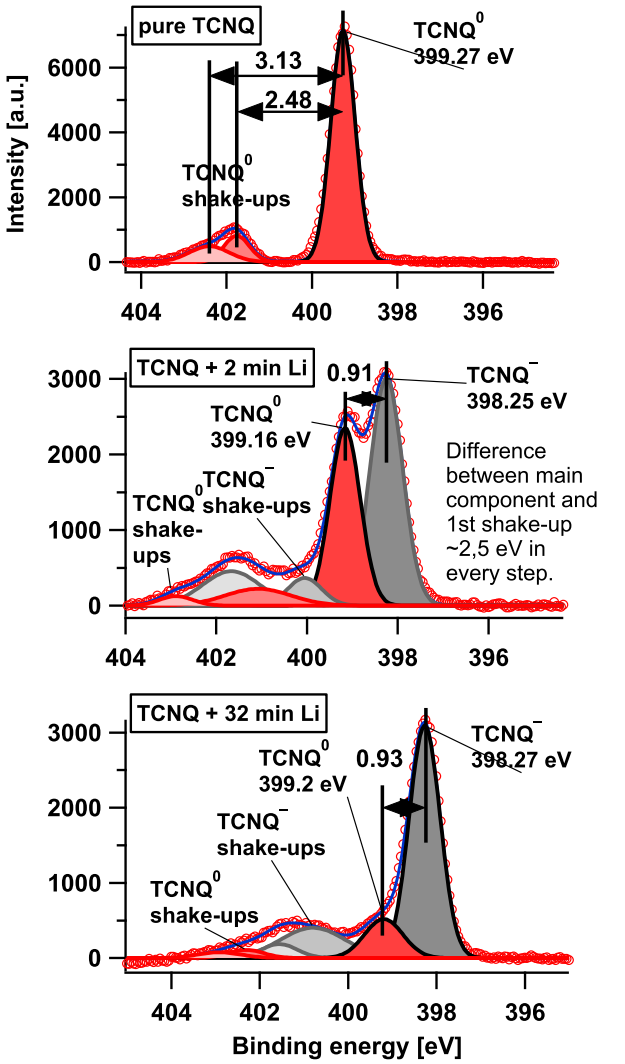

Fig. 4 N1s spectra of XPS measurements as superposition of neutral and negative charged TCNQ components for films of TCNQ without lithium and after intermediate and long exposure time. The shake-up peaks are devided into two peaks only due to easy fitting.

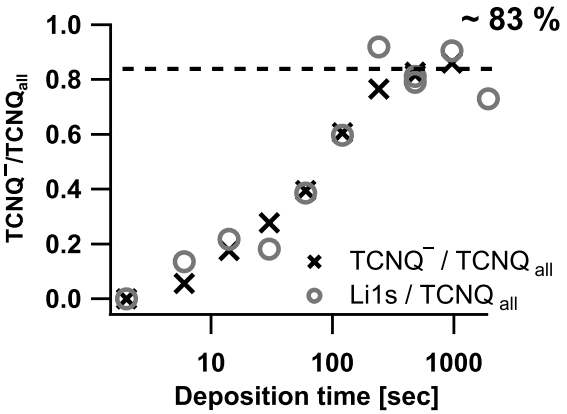

Fig. 5 Amount of Li and $TCNQ^-$ in the layer calculated by N1s seems to saturate at ca. 83%, i.e. approximately 17% of the TCNQ stays neutral. Calculations of Li1s/TCNQ(all) and $TCNQ^-$/TCNQ(all) result in similar values, indicating that one lithium atom leads to the formation of one $TCNQ^-$ molecule.

$TCNQ^-$. No significant variation in binding energy or shape is recognized for the TCNQ and $TCNQ^-$ spectra (i.e. signatures)

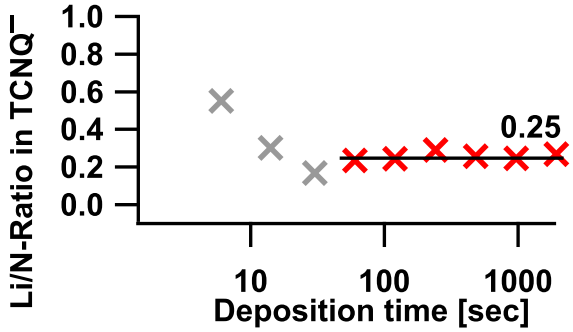

Fig. 6 Ratio of Li1s with respect to the negatively charged component of N1s in TCNQ. Grey: for short lithiation times the intensity of N1s(TCNQ⁻) and especially the Li1s peak were too low to calculate reasonable Li/N ratios (see Fig. 1, C and Fig. 3).

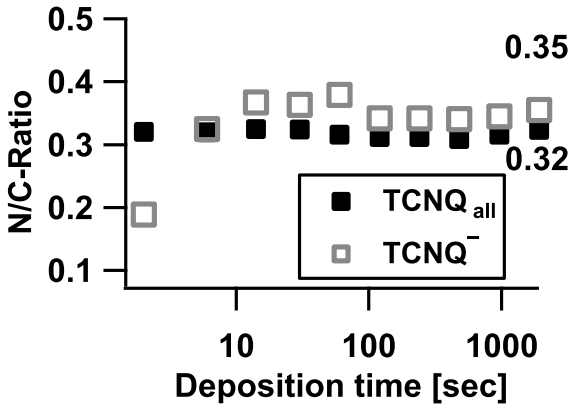

Fig. 7 Ratio of N1s/C1s for TCNQ(all) (=$TCNQ^0$ + $TCNQ^-$) and negatively charged $TCNQ^-$ component.

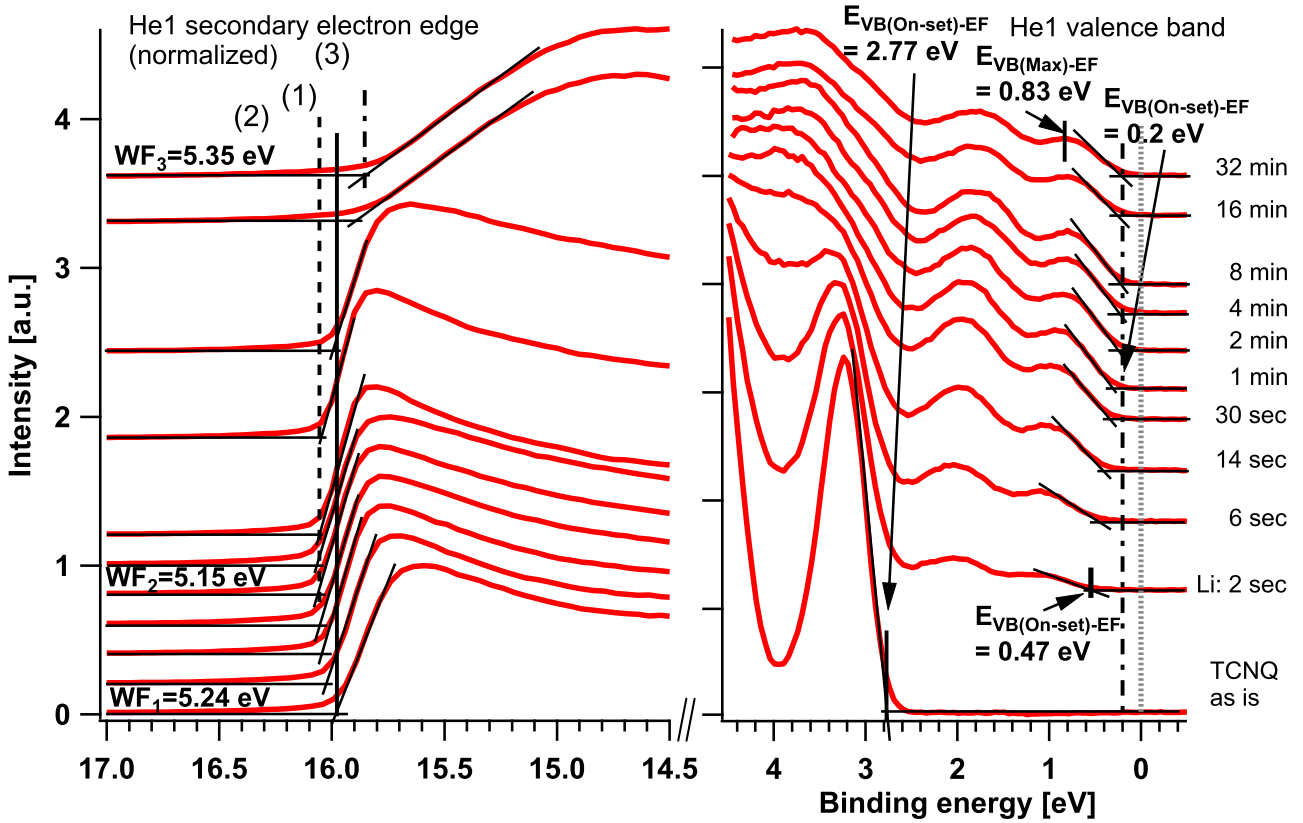

Fig. 8 UPS (HeI) measurements during deposition of Li on TCNQ. The bottom line represents pure TCNQ. The lines above match to the deposition times from XPS measurements. Left side: normalized secondary electron edge: the work function changes a little from 5.24 eV to 5.35 eV. Right side: valence spectra with values related to the Fermi energy at 0 eV: during intercalation the valence band (VB) on-set is decreased from 2.77 eV to 0.2 eV, due to the formation of two new valence band states in the original gap region.

with exposure time. Notably, however, the shape of $TCNQ^-$ in the C1s spectra significantly differs from TCNQ, while this is not the case in the N1s spectra. The additional modification of the spectra at higher binding energy is related to modifications of the satellite emissions.

In order to quantify the amount of TCNQ and $TCNQ^-$ with exposure time, N1s peak fits were performed. Fig. 4 shows exemplarily such fits for the TCNQ film without lithium, and after intermediate and long exposure time.

Fig. 5 presents the evolution of the lithium and $TCNQ^-$ fraction with exposure time. The amount of lithium was quantified by means of the Li1s signal (Fig. 1, C). The given values are only valid for the near-surface region, since photoelectron spectroscopy is a surface sensitive technique. We see a continuous increase and saturation at ca. 83%.

The evolution of the ratio of lithium to $TCNQ^-$ is shown in Fig. 6. After a continuous decrease of the ratio we find a loading of ca. 0.25 electrons per nitrogen atom with $TCNQ^-$ signature for long exposure times, according to one excess electron or one lithium ion per molecule. The initially high ratio we attribute to low intensities of the N1s($TCNQ^-$) and especially the Li1s peak which does not allow to calculate reasonable values (see Fig. 1, C

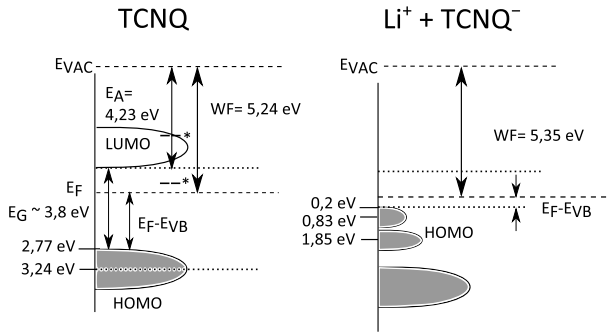

Fig. 9 Plot of UPS measurements of pure and intercalated TCNQ. Lindquist et al. reported the energy gap of TCNQ to be 3.5 eV [18]. For the electron affinity E_A of TCNQ different values can be found in literature [19] marked by stars. Kanai et al. found with inverse photoelectron measurements E_A of TCNQ to be 4.23 eV [20]. Taking this value into account we obtain in this experiment a bandgap of approximately 3.8 eV.

and Fig. 3).

The ratio of carbon to nitrogen, as evaluated by means of the area devided by the atomic sensitivity factor for the N1s and C1s signals both, remain constant during the whole experiment within the limitations of accuracy for quantification by XPS (Fig. 7). The mean value of 0.32 for the neutral and charged component nicely corresponds to the theoretical value of N/C = 4/12 = 1/3 for the TCNQ molecule ($C_{12}H_4N_4$).

3.2 UPS measurements

In addition to XPS measurements ultra violet photoelectron spectroscopy (UPS) has been performed.

The UPS measurements provide information about the energetic position of occupied electronic states (e.g. HOMO level, defect states), referenced to the Fermi level as well as vacuum level (by means of work function). Fig. 8 shows UPS measurements of TCNQ and Li-TCNQ, as obtained by the experiment.

For pure TCNQ the work function (left figure in Fig. 8) was determined to be 5.24 eV. The valence band (VB) on-set is 2.77 eV from the Fermi energy (right figure in Fig. 8). The work function remains almost constant during the experiment; with increasing exposure time first a slight decrease of work function is observed, followed by an increase to 5.35 eV. The changes in the valence band, also visible in Fig. 11, are pronounced. Upon lithium exposure, new states appear in the gap and the signature of the original HOMO states changes.

The results of the UPS measurements for pure and the last step of intercalation of lithium into TCNQ are summarized in Fig. 9.

4. Discussion

4.1 Insertion reaction

The spectra clearly show that upon exposure of the TCNQ film to lithium, lithium is inserted into the film and electrons are transferred to TCNQ molecules. We find no indication of a surface layer, such as metallic lithium or lithium oxide. Spontaneous insertion of alkali is a common phenomenon, because of the very negative electrochemical potential of alkali metals, which favours electron transfer to the TCNQ and the small dimensions of Li^+, which favours diffusion of the formed Li^+ into the $TCNQ^-$ layer. This already has been observed

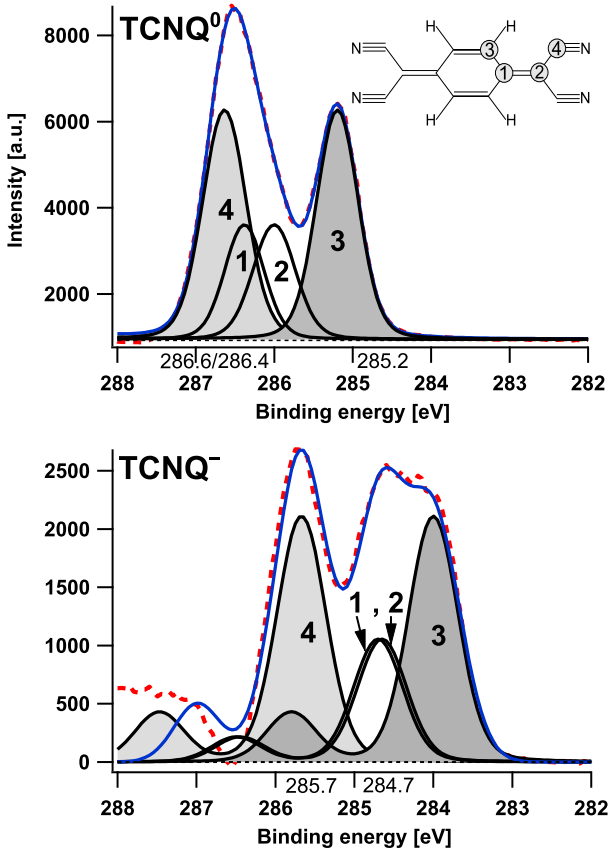

Fig. 10 C1s fit for $TCNQ^0$ (at the top, lowest C1s spectrum from Fig. 1) and $TCNQ^-$ (at the bottom, topmost C1s spectrum from Fig. 3) without the shake-up structure. The allocation of the carbon peaks fits to calculations by Miller et al. [23]. For $TCNQ^0$ the shake-up peaks are 2.6 eV separated from the photoemission there for they do not matter in the left picture. For $TCNQ^-$ this distance decreases so that we added a shake-up peak below peak 4 in the lower picture.

previously for lithium into TCNQ [4].

In the XPS spectra of the exposure sequence two distinctive signatures are present, which were denoted to $TCNQ^0$ and $TCNQ^-$. Literature indicates that the negatively charged $TCNQ^-$ is present as biradical dimers $[TCNQ_2]^{2-}$ [21] and we presume that this is also the case for our experiment. The formation of dimers involves a splitting of the bands [22] up to approximately 100 meV. In consideration of the energetic resolution of the used photoelectron spectrometer we are not able to distinguish between monomers and dimers. Therefore we keep on denoting the different spectral features $TCNQ^0$ and $TCNQ^-$ in the following discussion. We conclude that both TCNQ molecules and dimers are simultaneously present in the film, and that excess electrons are well localized on $[TCNQ_2]^{2-}$ dimers. This is in line with the formation of a small polaron usually observed for excess electrons on organic molecules [9].

In Fig. 10 a fitting of the C1s peak for $TCNQ^0$ and $TCNQ^-$ is proposed. The allocation of the peaks to certain carbon positions is based on calculations by Miller et al. [23]. The intensity ratio of the fits amounts 2:1:1:2 for $TCNQ^0$ and $TCNQ^-$ both. This ratio conforms to theoretical expectations from the structure of the TCNQ molecule.

There are only a few calculations for the charge density of the different carbon atoms in TCNQ with unfortunately inconsistent

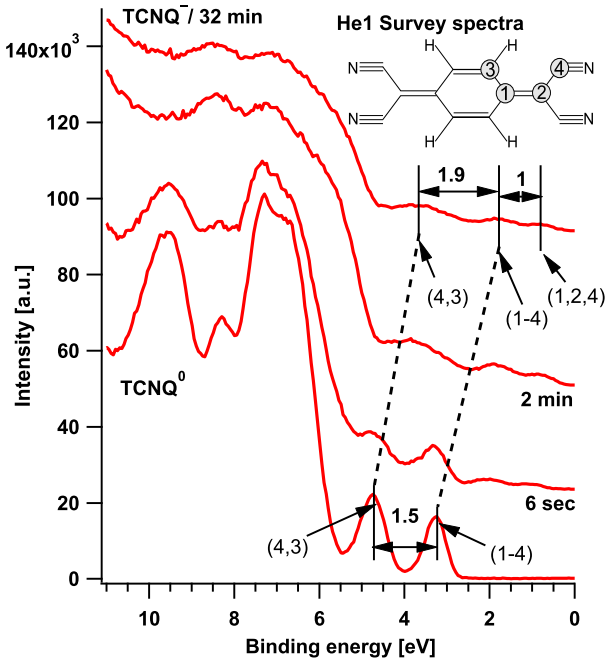

Fig. 11 Valence band structure from He1 survey spectrum. To clarify the changes in the valence band region only four steps are shown. The development of the valence bands during insertion of lithium into TCNQ is similar to the evolution reported by Lin and Spicer [4]: The two highest occupied molecular orbitals (HOMOs) of TCNQ (on the bottom side) shift upwards while their distance from each other increases a little from 1.5 eV to 1.9 eV. The peak at the lowest binding energy results from polaronic states. The numbers 1 to 4 in brackets mark the carbon atoms which contribute to a certain valence orbital [4,27].

results [23,24]. Miller et al. and Jonkman et al. have consistent calculations for the relative position of peak 1 and 4 on the left side of the binding energy scale. So peak 2 and 3 offer some uncertainty in the calculation of their binding energy. For $TCNQ^0$ also other fits are suggested with accordance with peak 3 [25]. In $TCNQ^-$ peak 1 and 2 shift to the right side until they are nearly overlapping. The binding energy of the C1s peaks of the proposed fits of $TCNQ^0$ and $TCNQ^-$ are shown in Table 1.

Table 1 Binding energies of C1s peak in $TCNQ^0$ and $TCNQ^-$. C_2 is typed italic due to inconsistent calculations.

	$TCNQ^0$ [eV]	$TCNQ^-$ [eV]	Shift [eV]
C_1	286.4	~284.7	-1.7
C_2	*286.0*	*~284.7*	*-1.3*
C_3	285.2	284.0	-1.2
C_4	286.6	285.7	-0.9

In spite of partly inconsistent calculations the XPS measurements indicate that the additional charge from the valence electron of the added lithium atoms are localized at C_1 to C_3 and less at C_4, which is showing the smallest shift towards lower binding energies. Although the calculations of the neutral and the reduced form of TCNQ have only 50 % compliance the C1s fits match well to the experimental XPS detail spectra.

The UPS measurements of the valence band region in section 3.2 reveal that the valence electron of lithium is transferred to the

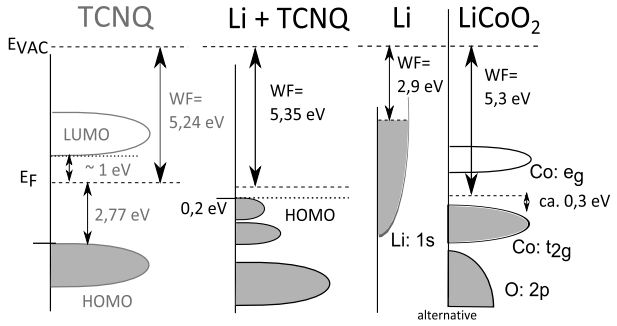

Fig. 12 Comparison of the work functions of pure and lithium intercalated TCNQ, lithium and $LiCoO_2$ for approximation of electrode potentials. Surface potentials of the different materials are not considered in this procedure. The work function of metallic lithium is 2.9 eV [35]. Orbital structure of $LiCoO_2$ extracted of [36] and distance between Fermi level and valence band for $LiCoO_2$ from [37].

organics forming a small polaron. This results in a shift of the original LUMO downwards below the Fermi level. Due to electron-electron repulsion the HOMO at 3.2 eV and the 1.5 eV separated state (in Fig. 11) shift upwards [4,26]. According to results of Lin et al. their distance increases slightly to 1.9 eV.

The new features continuously evolve during the experiment. The presence of a gap state and related changes in the original HOMO level were reported before [28]. The gap states are attributed to the two highest singly- and doubly-occupied π orbitals of negative charged $TCNQ^-$. The new highest occupied molecular orbital (HOMO) has the maximum intensity at 0.83 eV and the on-set lies at 0.2 eV.

Just like the fitting of the C1s emission line the valence band region in Fig. 11 should give evidence to the distribution of additional valence electrons on the TCNQ molecule. Since all carbon atoms (marked Fig. 11 with numbers 1 to 4 in brackets) contribute to nearly every valence band peak the distribution of the electron over different carbon atoms in $TCNQ^-$ can hardly be distinguished. For the carbon atom C_4 we find both for the core level line and the valence peak at 4.8 eV a shift of approximately 0.9 eV towards lower binding energies. As well the feasibility to determine the position of the lithium cation in the environment of the TCNQ molecule seems not to be possible. Insertion of only electrons into TCNQ [29] or lithium atoms results in similar spectra for XPS and UPS so that it is questionable if any position related effect of the lithium cation is detectable using photoelectron spectroscopy at all.

Calculating the ratio between the lithium and the nitrogen signal intensity we find an average of one electron per four nitrogen atoms associated with negatively charged $TCNQ^-$. This indicates that the excess charge is delocalized over the entire molecule (or dimer, respectively), in agreement with numerical simulations [30]. Notably the change of shape of the C1s signal upon electron uptake indicates that delocalization is not fully homogeneous, however.

The carbon and nitrogen stoichiometry is not altered by lithiation and we observe no indication of a decomposition reaction.

The maximum loading in the experiment was one lithium atom per TCNQ molecule. Hanyu et al. [2] transferred two electrons per TCNQ molecule electrochemically. We attribute the lower level of lithiation to continuous diffusion of lithium to the volume of the film beyond the range of the detection limit of surface

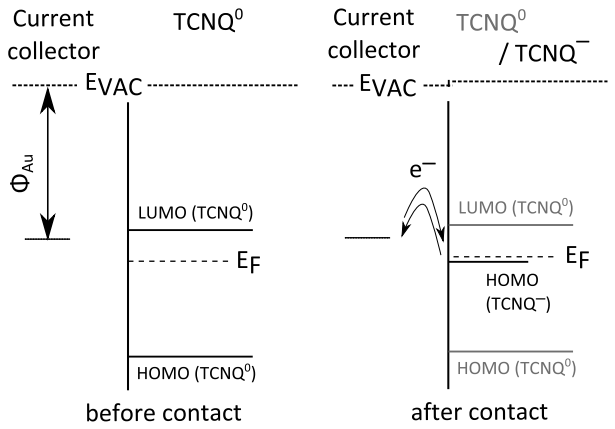

Fig. 13 Bi-directional electron transport at the interface between current collector and $TCNQ^-$. Work function of Au adopted from [35]. Braun et al. reported about the integer charge transfer at organic/metal interfaces [12].

sensitive XPS.

4.2 Electrode potential

The electrode potential of a lithium insertion compound is determined by the lithium chemical potential. Usually, for inorganic compounds, the contributions of electrons and ions to the lithium chemical potential may be separated in good approximation [15], and the electronic contribution, i.e. the electron chemical potential, dominates the electrode potential by far (see e.g. [10]). Approximation of the electron chemical potential can proceed via the work function upon disregard of any surface potential. In the following, we briefly discuss the relation of the work function to electrode potential for TCNQ as well as lithium cobalt oxide ($LiCoO_2$) and lithium, as has been done before for inorganic lithium intercalation thin film electrodes [31].

The work function of both the pure and lithiated TCNQ film is close to 5.3 eV (see Fig. 12). This value is quite comparable to the work function of a $LiCoO_2$ thin film, for which we also find ca. 5.3 eV [32]. For the fully lithiated $LiCoO_2$ a value of 3 V vs. Li/Li^+ is typically quoted as electrode potential [33]. On basis of the work function difference, i.e. neglecting any differences in lithium ion chemical potential or surface potential, a similar value is expected for the TCNQ electrode. Indeed, the value corresponds reasonably well to the value reported for the second discharge plateau (2.4-2.6 V) by Tobishima et al., as obtained for a battery containing TCNQ and acetylene black as cathode and lithium as anode [6]. Notably, application of this simple procedure to evaluate the electrode potential of TCNQ directly with respect to lithium (work function 2.5-2.9 eV [34,35]) yields a potential of 2.8-2.4 V vs. Li/Li^+ which fits quite well both for $LiCoO_2$ and TCNQ.

In inorganic intercalation compounds like Li_xCoO_2 charge compensation is mostly sustained by localized, d-orbital derived states of the transition metal. Nevertheless, the degree of lithiation, i.e. the population of electronic states and ionic states, has some influence on the band structure, demonstrating that charge compensation is a solid-state phenomenon. These effects remain small, however, compared to polaronic effects in organic materials. The formation of polarons in the present case, and for organic materials in general, significantly shifts the electrode potential to a more positive value (i.e. shifts the Fermi energy downwards). Without polaron formation, i.e. with a rigid energy-level structure of TCNQ, the excess electrons would populate states at the LUMO-energy, corresponding to n-doping with a significant shift of Fermi-level upwards.

The electrode potential of lithium insertion compounds depends often on the degree of lithiation [10,38]. The electrode potential of the insertion compound then becomes more negative with increasing lithium content. This evolution of the electrode potential is usually dominated by electronic effects, i.e. population of electronic states and changes in the electronic structure. In the case of TCNQ no upward shift of the Fermi level is observed with lithiation due to polaron formation. This behavior is in line with a plateau in the charge/discharge curve.

4.3 Kinetic aspects

For the operation of an insertion electrode both electron and Li-ion conductivity in the insertion compound are important, as well as electron and Li-ion transfer resistances at the interfaces to current collector and electrolyte. In contrast to applications of semiconducting organic compounds in electronics, bi-directional flow of electrons has to be considered: depending on operation (charge or discharge), electrons are inserted or extracted via the interface to the current collector while ions are transferred through the electrode electrolyte interface. In the following, we briefly discuss electron conduction effects on basis of the presented results and the known phenomena related to conducting organic compounds.

During intercalation of lithium into the TCNQ layer the valence electron of lithium is transferred to the organics forming a small polaron. The typical charge-carrier localization time is several orders of magnitude greater than the relaxation time for electronic polarization of the surrounding lattice molecules [39]. With regard to electron conduction inside a TCNQ electrode polaron transfer via a hopping mechanism has to be considered. That necessitates the electrons to overcome at least half of the polaron binding energy [40], corresponding to an activation energy of ca. 0.6 eV for electron conduction in the present case.

Electron transport over the interface with the current collector strongly depends on how interface formation proceeds, i.e. whether the formation takes place under charge transfer and interfacial dipole formation, or not. Usually, (integer) charge is transferred at such weakly interacting metal-organic interfaces if the work function of the metal is smaller than the (vacuum-referenced) energy of the negatively charged polaron state, resulting in an alignment of metal Fermi-level and polaron energy-level [12]. In this case, electron transfer resistance is low (usually ohmic), presumably also for transfer from organic to metal (see Fig. 13). Notably, in the case that interface formation takes place without such charge separation, i.e. formation of a dipole layer, electron transfer resistance depends on the direction of transfer and strongly on the type of metal.

5. Conclusion

Lithium was gradually inserted into a TCNQ thin film from the gas phase. The charge compensation was monitored by X-ray and ultra-violet photoelectron spectroscopy. For the first time we report measurements of the work function and show XPS spectra of all involved core emission lines N1s, C1s, Li1s as well as the valence band for the different contents of lithium in TCNQ.

The results confirm that the insertion of lithium takes place under polaron formation. There is no change in composition of the TCNQ, we thus find no indication of a degradation of TCNQ upon lithium insertion within the limits of the experimental technique. During the intercalation experiment the stepwise formation of the charged $TCNQ^-$ component could be observed. The results demonstrate that the excess electrons are well localized on TCNQ species, presumably forming $[TCNQ_2]^{2-}$ dimers, and are consequently in line with an integer charge transfer.

In addition to the insertion reaction, electrode potential and kinetic aspects relevant for application in batteries are discussed. The polaron formation affects the electrode potential beneficially. During the intercalation of lithium into TCNQ, the Fermi level remains nearly constant, i.e. the work function and the electrode potential hardly change, explaining the plateau in the charge/discharge curve. However the binding energy of a polaron is expected to have adverse effects on the electron conduction of the material.

Acknowledgement:

This research is funded by Novaled AG, Germany and Sächsische Aufbaubank, Germany, under the project 100085111. We also would like to acknowledge funding by the BMBF (Federal Ministry of Education and Research).

References

Department of Materials Science, Surface Science Division, Darmstadt University of Technology, Jovanka-Bontschits-Str. 2, D-64287, Darmstadt, Germany. Email: rprecht@surface.tu-darmstadt.de

1 B. Scrosati, *Polymer electrodes*, Cambridge University Press, Cambridge, 1994, vol. 5.

2 Y. Hanyu and I. Honma, *Sci. Rep.*, 2012, **2**, 453, <Go to ISI>://MEDLINE:22693655.

3 B. Scrosati and J. Garche, *Journal of Power Sources*, 2010, **195**, 2419–2430.

4 S. F. Lin, W. E. Spicer and B. H. Schechtman, *Physical Review B*, 1975, **12**, 4184–4199, http://link.aps.org/doi/10.1103/PhysRevB.12.4184.

5 P. Nielsen, A. J. Epstein and D. J. Sandman, *Solid State Communications*, 1974, **15**, 53–58.

6 S.-i. Tobishima, *J. Electrochem. Soc.*, 1984, **131**, 57.

7 B. C. Melot and J.-M. Tarascon, *Acc. Chem. Res.*, 2013, **46**, 1226–1238.

8 J. B. Goodenough and Y. Kim, *Chem. Mater.*, 2010, **22**, 587–603.

9 G. Horowitz, *Journal of Materials Chemistry*, 1999, **9**, 2021–2026, http://dx.doi.org/10.1039/A902242B.

10 D. Tonti, C. Pettenkofer and W. Jaegermann, *J. Phys. Chem. B*, 2004, **108**, 16093–16099.

11 G. Horowitz, *Advanced Materials*, 1998, **10**, 365–377, http://dx.doi.org/10.1002/(SICI)1521-4095(199803)10:5<365::AID-ADMA365>3.0.CO;2-U.

12 S. Braun, W. R. Salaneck and M. Fahlman, *Adv. Mater.*, 2009, **21**, 1450–1472.

13 a) R. e. a. Grant, **1987**. b) A. e. a. Klein, *Bunsen-Magazin*, 2008, **10**, 124–139. c) R. Schlaf, A. Klein, C. Pettenkofer and W. Jaegermann, *Phys. Rev. B*, 1993, **48**, 14242–14252. d) C. Pettenkofer, W. Jaegermann, A. Schellenberger, E. Holub-Krappe, C. Papageorgopoulos, M. Kamaratos and A. Papageorgopoulos, *Solid State Communications*, 1992, **84**, 921–926.

14 Q.-H. Wu, A. Thißen and W. Jaegermann, *Surface Science*, 2005, **578**, 203–212.

15 W. Jaegermann and D. Tonti, *New Trends in Intercalation Compounds for Energy Storage. Proceedings of the NATO Advanced Study Institute on New Trends in Intercalation Compounds for Energy Storage*, 2002.

16 R. Hausbrand, D. Becker and W. Jaegermann.

17 W. Jaegermann, C. Pettenkofer, A. Schellenberger, C. A. Papageorgopoulos, M. Kamaratos, D. Vlachos and Y. Tomm, *Chemical Physics Letters*, 1994, **221**, 441–446, http://www.sciencedirect.com/science/article/pii/000926149400286X.

18 J. M. Lindquist and J. C. Hemminger, *Journal of Physical Chemistry*, 1988, 1394–1396, <Go to ISI>://WOS:A1988M716500005.

19 a) C. E. Klots, *J. Chem. Phys.*, 1974, **60**, 1177. b) K. Imai, S. Hatano, A. Kimoto, J. Abe, Y. Tamai and N. Nemoto, *Tetrahedron*, 2010, **66**, 8012–8017.

20 K. Kanai, K. Akaike, K. Koyasu, K. Sakai, T. Nishi, Y. Kamizuru, T. Nishi, Y. Ouchi and K. Seki, *Appl. Phys. A*, 2009, **95**, 309–313.

21 a) I. Shirotani and N. Sakai, *Journal of Solid State Chemistry*, 1976, **18**, 17–25, http://www.sciencedirect.com/science/article/pii/0022459676900748. b) M. J. Rice, V. M. Yartsev and C. S. Jacobsen, *Phys. Rev. B*, 1980, **21**, 3437–3446, http://link.aps.org/doi/10.1103/PhysRevB.21.3437. c) V. Dong, H. Endres, H. J. Keller, W. Moroni and D. Nöthe, *Acta Crystallogr B Struct Crystallogr Cryst Chem*, 1977, **33**, 2428–2431.

22 J. J. Novoa, P. Lafuente, R. E. Del Sesto and J. S. Miller, *CrystEngComm*, 2002, **4**, 373.

23 J. S. Miller, J. H. Zhang, W. M. Reiff, D. A. Dixon, L. D. Preston, A. H. Reis, E. Gebert, M. Extine and J. Troup, *The Journal of Physical Chemistry*, 1987, **91**, 4344–4360, http://dx.doi.org/10.1021/j100300a028.

24 a) H. T. Jonkman and J. Kommandeur, *Chemical Physics Letters*, 1972, **15**, 496–499. b) V. E. Klimenko, *Theor Exp Chem*, 1985, **20**, 567-570, http://dx.doi.org/10.1007/BF00522453.

25 C. Hein, PhD, Technische Universität Darmstadt, 2012.

26 C. Tengstedt, M. Unge, M. de Jong, S. Stafström, W. Salaneck and M. Fahlman, *Phys. Rev. B*, 2004, **69**.

27 F. Herman, W. E. Rudge, I. P. Batra and B. I. Bennett, *Int. J. Quantum Chem.*, 1976, **10**, 167–181.

28 a) J. Giergiel, S. Wells, T. Land and J. C. Hemminger, *Surface Science*, 1991, **255**, 31–40. b) B. H. Schechtman, S. F. Lin and W. E. Spicer, *Physical Review Letters*, 1975, **34**, 667–670, <Go to ISI>://WOS:A1975V812100011.

29 S. Braun, X. Liu, W. Salaneck and M. Fahlman, *Organic Electronics*, 2010, **11**, 212–217.

30 Z.-J. Li, Z.-R. Li, F.-F. Wang, F. Ma, M.-M. Chen and X.-R. Huang, *Chemical Physics Letters*, 2009, **468**, 319–324.

31 Q.-H. Wu, A. Thissen and W. Jaegermann, *Applied Surface Science*, 2005, **250**, 57–62.

32 D. Ensling, Dissertation, Technische Universität Darmstadt, 2006.

33 A. Thißen, D. Ensling, M. Liberatore, Q.-H. Wu, F. J. Fernandez Madrigal, M. S. Bhuvaneswari, R. Hunger and W. Jaegermann, *Ionics*, 2009, **15**, 393-403, http://dx.doi.org/10.1007/s11581-009-0339-z.

34 P. Anderson, *Phys. Rev.*, 1949, **75**, 1205–1207.

35 L. Bergmann and C. Schaefer, eds., *Lehrbuch der Experimentalphysik Band 6, Festkörper*, Walter de Gruyter, 2005.

36 M. Czyżyk, R. Potze and G. Sawatzky, *Phys. Rev. B*, 1992, **46**, 3729–3735.

37 D. Ensling, G. Cherkashinin, S. Schmid, S. Bhuvaneswari, A. Thissen and W. Jaegermann, *Chem. Mater.*, 2014, **26**, 3948–3956.

38 R. A. Huggins, *Advanced batteries. Materials science aspects*, Springer, New York, [London], ©2009.

39 R. Farchioni and G. (. Grosso, *Organic Electronic Materials. Conjugated Polymers and Low Molecular Weight Organic Solids*, Springer Berlin Heidelberg, Berlin, Heidelberg, 2001, Vol. 41.

40 M. A. Baldo and S. R. Forrest, *Phys. Rev. B*, 2001, **64**, 85201, http://link.aps.org/doi/10.1103/PhysRevB.64.085201.